Paper No.
00046

CORROSION 2000

SURFACE CHEMICAL AND MORPHOLOGICAL CHANGES IN CORROSION PRODUCT LAYERS AND INHIBITORS IN CO_2 CORROSION IN MULTIPHASE FLOWLINES

S. Seal, K. Sapre and V. Desai

Advanced Materials Processing & Analysis Center (AMPAC)
and
Mechanical, Materials, and Aerospace Engineering (MMAE),
Eng. 381, 4000 University Blvd
University of Central Florida, Orlando, Fl-32816

M. Gopal and W. P. Jepson

[b] Institute for Corrosion and Multiphase Technology
Ohio University, 340 1/2 West State Street
Athens, OH 45701

ABSTRACT

This communication reports the effects of multiphase flow on the corrosion products formed on the surface of 1018 C-steel coupons in oil and gas lines. The main objective of this paper is to understand the effects of multiphase flow (full pipe and slug flow Fr. No. 6 and 9 at various flow and oil-water mixtures) on the morphology and the porosity of the C-steel coupon subjected to a horizontal test loop. The corrosion product layer formed on the surface of the steel coupons were analyzed using Scanning Electron Microscopy (SEM), Electron Dispersive Spectroscopy (EDS), X-ray mapping, Atomic Force Microscopy (AFM) and X-ray Photoelectron Spectroscopy (XPS). Detailed porosity calculation has been carried out using metallographic software. The porosity increases as the flow velocity is increased. The corrosion product layer is primarily made of iron carbonate crystals along with Na and Cl as indicated by EDS measurements. Detailed XPS analysis show the deterioration of inhibitor film as the flow is increased from full pipe (Fr = 0) to slug flow (Fr = 6). XPS shakeup satellite lines in the N (1s) spectra have been useful in the analysis.

Keywords: Imidazolines, Multiphase flow, XPS, Satellite peaks, C-Steel, AFM

INTRODUCTION

Internal corrosion due to carbon dioxide (CO_2) in oil and gas pipelines is a very common occurrence in petroleum industries.[1] CO_2 gets introduced into the system through the water that is pumped into the oil wells to decrease the viscosity of the oil to facilitate easy and faster recovery. However, the presence of CO_2 in the system proves to be the prime cause of corrosion in the C-steel pipelines. The dissolved CO_2 reacts to form carbonic acid (H_2CO_3), which is the initiating step for corrosion to progress in the pipelines.[2] There are various factors that contribute to CO_2 corrosion in C-steel pipelines amongst which the effect of flow is one which causes the most damage to the lines. The corrosion reaction leads to the formation of iron carbonate ($FeCO_3$) as a corrosion product that tends to settle on to the surface of the steel as it corrodes. Thus, it influences the rate of corrosion taking place in the pipelines.[3, 4] The ability of this corrosion product layer to stay attached to the surface of the C-steel is dependent to a great extent on the oil and gas velocities in the lines. If the flow regime is that of a slug flow then its turbulent nature does not allow the corrosion layer to settle down on the surface. On the other hand if it's a full pipe then the corrosion product layer is quite significant.[4, 5] Corrosion of C-steel pipelines has prompted the consideration of a corrosion inhibitor program in various oil fields around the world. The importance and usefulness of oleic imidazoline inhibitors in oil and gas pipelines has been studied in detail by several researchers.[6, 7, 8, 9] Most of these commercial inhibitors have organic polar molecules that absorb on to the metal surface and form a protective film barrier.

The basic aim of this paper is to analyze the corrosion product layer by using various analytical techniques. Effect of flow on porosity is also discussed. Preliminary AFM measurements were carried out to confirm the variation in topography shown in the SEM micrographs. Furthermore, this communication represents a detailed surface chemical study of C-steel coupons in the presence of oleic imidazoline inhibitor in full pipe and slug flow conditions.

EXPERIMENTAL CONDITIONS

The 1018 C-steel specimens (0.437 in diameter and 0.126 in thickness) are exposed to a high-pressure horizontal loop at the "Center for Corrosion in Multiphase Systems" at Ohio University. All coupons were polished, cleaned in DI water and then flush mounted at the bottom of the pipeline. The coupons were exposed to slug flow and full pipe flow in a horizontal test loop at various flow conditions listed below:

Test Matrix

	FLOW TYPE	CONDITION
Sample 1:	Full pipe	Velocity = 0.55 m/s (24 hours, 100% water cut)
Sample 2:	Full pipe	Velocity = 1.1 m/s (24 hours, 100% water cut)
Sample 3:	Full pipe	Velocity = 1.5 m/s (24 hours, 100% water cut)
Sample 4:	Slug flow	Froude No. 6 (5 hours, 100% water cut)
Sample 5:	Slug flow:	Froude No. 9 (5 hours, 100% water cut)
Sample 6:	Full pipe	Velocity = 1 m/s (100% water cut)
Sample 7:	Slug flow	Froude No. 6 (100% water cut)
Sample 8:	Slug flow	Froude No. 9 (100% water cut)
Sample 9:	Slug flow	Froude No. 9 (80% water cut)
Sample 10:	Full pipe	Velocity = 0.55 m/s (100 % water cut + Inhibitor)
Sample 11:	Slug flow	Froude No. 6 (100 % water cut + Inhibitor)

Porosity measurements were carried out on sample 6, 7, 8, 9. The liquid composition chosen in this case are 0% and 20% oil by volume and seawater. The percent porosity of the sample varies depending on the flow type to which the sample is exposed.

For inhibitor studies, a mixture of ASTM substitute seawater and oil of viscosity 2 centipoise is used in the liquid phase with carbon dioxide in the gas phase. CO_2 is introduced into the system immediately before the test section. Both Sample10 and Sample11 are studied in presence of oleic imidazoline inhibitor.

All coupons were stored under vacuum in sealed containers, and were transferred to the pucks in an inert argon glovebox to make sure that moisture or air does not contaminate the surface.

Using SEM & EDS the coupons were analyzed for the nature of the corrosion product topography and its chemical constituents. Furthermore, AFM measurements were taken on samples 1, and 5 to monitor the effect of flow velocity on topography in atomic scale.

Detailed surface chemical analysis was performed using a 5400 PHI ESCA (XPS) spectrometer using AlKα X-radiation at 350 watts. The base pressure was 10^{-10} torr during analysis. The spectrometer scale was calibrated using gold ($4f_{7/2}$) = 84 + 0.2 eV. Any charging shifts produced were removed by using a binding energy scale by fixing the C(1s) binding energy (adventitious carbon) at 284.6 eV.[10]

RESULTS AND DISCUSSION

SEM, EDS (Sample 1-5) and AFM (Samples 1 & 5) analysis of the corrosion specimens reveal certain features from which it can be concluded that:

Full pipe

Figure 1 (a, b, c, d) represents the SEM micrographs of full pipe flow samples exposed to various flow velocities. Figure 1 a (0.55 m/s) shows distinct grain boundaries with minimal corrosion product on the surface. As the flow velocity is increased (Figure 1 b) 1.1 m/s) the amount of corrosion product is increased and the surface is fully covered with $FeCO_3$ crystals in the sample exposed to a velocity of 1.5 m/s (Figure 1 c and d). This result is unique, because it is expected that a more serrated type corrosion product layer would be seen in this sample, because the flow velocity is increased. Careful observation of the dense structure reveals the stacking of the iron carbonate crystals, just like a deck of cards arranging at an angular fashion (Figures 1 c & d). At this velocity, iron carbonate crystals might have cleaved into smaller crystals and preferentially arranged along a preferable plane. Preferential stacking of these product layer will make a corrosion product film more compact and thus a lower corrosion rate is more expected and is confirmed by Hong (1999),[11] with EIS measurements on these coupons. His observation showed that the porosity at 1.3 m/s liquid velocity is lower than that at 0.55 m/s. This may be due to the presence of secondary layer on the top of the primary surface caused due to the recrystallization of the iron carbonate.[12] This secondary layer is more densely packed in nature. The smaller crystals give better protection due to higher crystallinity than the larger crystals.[13]

Slug flow

Figure 2 (a) and (b) shows SEM micrograph (Froude 6) along with EDS spectrum. Lesser amount of Na and Cl is found in the slug flow condition as compared to the full pipe flow. Extensive corrosion is

seen on the surface with dispersed iron carbonate crystals that show distinct holes in the surface. However, this is not pitting corrosion, it might be some pre-existing hole on the surface. The size of crystals is less, an effect of the turbulent flow, shearing the surface. The exposure of the metal surface acts as fresh nucleating sites for further corrosion.

As the Froude Number is increased to 9, the surface captures the signature of bubble impact (see Figure 3 a). Part of the corrosion product is removed leaving behind the impact crater due to the bubble. This maybe due to the collapsing bubbles created by pressure changes across the surface. When the bubbles land on the surface and collapse, the repeated pressure impacts are sufficient to erode the surface. Removal or thinning of protective surface films allows more rapid corrosion of the underlying metal, which forms more of the erodible porous corrosion product film on the surface, as seen in Figure 3 b. The layer of the corrosion product film is so small that its visibility using optical microscope (OM) is very difficult. Extreme high velocities and shear rates remove the possibility of formation of a protective film on the surface indirectly increasing the corrosion in the process.

Porosity measurements

Values of porosity of the corrosion product film are needed for insertion into models for corrosion rate calculation. Diffusion coefficients can be estimated by several methods, e.g. EIS, but validation and calibration are difficult since there are little data on these or by porosity under multiphase flowing conditions. Both SEM and porosity measurements were carried out in samples 6, 7, 8, 9 (see Figure 4). In full pipe flow (seawater), the surface appears to be smooth with very little nodular type growth (mushroom type). EDS spectrum of the surface primarily shows Fe and C with a little trace of Mn and O. The x-ray maps of the surface (see Figure 5) reveal the evidence of such iron carbonate formation. From the images of the surface on these photographs, an analysis was conducted using metallurgical software developed by the Bulgarian Academy of Sciences, Bulgaria. The image analysis package examined the shape and size of the imperfections in the surface and is calibrated to a known porosity from a standard sample. From these, a value of the porosity is obtained. While calculating the percent porosity special consideration is taken for the aspect ratio, hole area, roundness etc. Since the corrosion product layer is thin (see later), the values of porosity calculated from the surface orientation should provide a realistic estimation of the true porosity.

Based on these parameters, the % porosity was calculated for the following samples: Full pipe flow at a velocity of 1.1 m/s, and slug flow with Froude numbers 6 and 9 at 100% water cut, together with slug flow with Froude number 9 at 80% water cut.

While calculating porosity, 3 basic objects that were seen on the images are:

- black assumed to be pores
- gray as matrix material &
- white (corrosion product ~ carbides (may be))

In Figure 4, the full pipe flow sample with 100% water cut shows a compact nature with no grain boundaries visible. Some parts of the sample show black spots, which were assumed to be pores and made upto ~5% of the total surface. As seen from the image the black spots seem to be concentrated around the white spots suggesting a relationship between the two. It is possible that the white spots (mixed iron carbides and iron carbonates) might in some way influence the formation of pores (black spots). Fewer amounts of white spots on the surface would mean that the surface is more homogenous and even.

It can be seen that the aspect ratio of the holes does not change much with values of 2.4 – 2.5 being reported. However, as the flow changes from full pipe flow to slug flow, the mean hole size changes by at least a factor of 10. This suggests that much larger holes are found at in slug flow and this is probably due to the bubble impact. The porosity calculated for the full pipe flow (100% water cut) is about 6% (refer to the table 1), which indicates that the surface is not very porous in nature. Slug flows are inherently associated with high turbulence and the corrosion product layer is much thinner and therefore more corrosion can take place. For slug flow (Froude No.6, 100% water cut) the surface seems to be rougher with larger holes and cracks in it. The calculated porosity is 24%, which is a 4-fold increase from the full pipe flow. An increase in the percent porosity of the sample is attributed to the increased mean hole diameter of the pores along with the mean roundness. The holes are now more elliptical than circular in shape. At higher Froude numbers, the % porosity further increases as now the surface starts to appear more loosely attached to the substrate. The percent porosity for this value of Froude No.9 is 30 %. A drop in the mean roundness would suggest that the holes are more circular. The % porosity rises further with the introduction of oil. At a water cut of 80 %, at Froude No. 9, the porosity is 31%. The mean roundness is also seen to decrease a little which would mean more circular pores. The surface seems to be covered with white spots along with large black cracks. The gray matrix is not seen at all The increase in corrosion rates are associated with high porosity values due to enhanced diffusion of the reactive species through the pores at the metal surface at higher Froude numbers. In presence of oil, the increase in porosity is an indication of more corrosion as compared to the one at the 100% water cut under similar flow conditions thus destabilizing the corrosion product layer.

AFM measurements

Figure 6 (a and b) shows the 2D and 3D AFM images of full pipe samples exposed to 0.55 m/s. Stepped type morphology is observed with stacked iron carbonate crystals. The 3D image did not show much amplitude variation in the topography. Roughness measurements were carried out using a DI300 AFM in contact mode. The roughness results are normally expressed as the root mean square roughness (Rq) which is the standard deviation of the Z values (perpendicular to the X-Y plane) in a given area (scan area size analyzed = 5 microns) and the mean roughness (Ra) which is the arithmetic averages of the deviations from the center plane. The RMS value for V = 0.55 m/s on a scan area of 5 microns at different spots on the surface ranges between 146.79 nm and 232.52 nm. The Ra values for the same sample are between 119.74 nm and 184.82 nm.

Figure 7 (a and b) represents similar 2D and 3D AFM images of Fr. 9 sample. Interesting to note that the surface did not show much crystals and at regions valleys are seen. The 3D AFM image definitely show amplitude variation indicating a much rougher surface, an indication of high corrosion rate. The RMS value on the surface range as: Rq = 555.08 to 560.91 and the Ra = 453.86 to 473.12, which is much higher than the full pipe sample.

Application of Surface Analytical techniques in Multiphase Corrosion:

An important aspect of the surface film formation and breakdown mechanism depends on the surface chemistry of the passive films. A detailed characterization of the surface film will provide fundamental knowledge of the elemental composition and the binding state of various cationic and anionic species. CO_2 corrosion of carbon steel contains various iron corrosion products: iron carbonate ($FeCO_3$), wustite (FeO), hematite (Fe_2O_3) and magnetite (Fe_3O_4). With the help of XPS, one can distinguish which corrosion products are present because XPS can reveal chemical state information from a specimen on the basis of chemical shift.

XPS reports by Heuer and Stubbins (1998) indicate the XPS C(1s), Fe(2p) and O(1s) photoline corresponds to 289.4 eV, 710.2 eV and 531.9 eV for a standard and pure iron carbonate crystal.[14] In the seawater condition, the iron carbonate signatures (Figure 8 a, b, c: C 1s binding energy at 289.2 - 289.5 eV) are revealed. It is observed that the intensity increases as the flow is increased (indicating top surface removal), whereas the intensity of the carbonate signal is more or less uniform as the slug flow is increased in the seawater+20% oil mixtures (Figure 8 d, e, f). Nevertheless the carbonate species present on the surface is minimal and it might be due to the decomposition of iron carbonate following oxidation in presence of oxygen and air. Presence of C=O species (C1s binding energy at 288.4 eV) are observed on the steel surface subjected to slug flow.

Effect of Inhibitor

Detailed XPS was performed on the steel coupons (Sample 10 and 11) to identify the chemical nature of the inhibitor as a function of flow. XPS survey spectra from Sample 10 and 11 are shown in Fig.9 (a) and Fig.9 (b). The nitrogen content in the slug flow decreases to 3% from 6% in the full pipe flow (S-10). This indicates the removal of inhibitor, as the Froude number is increased from 0 to 6 number. Also a decrease in Fe content in Sample 10 and the presence of Na and Cl is an indication of NaCl presence. This was not detected in our early EDX measurements, which clearly separates the usefulness of bulk vs. surface analytical techniques. Furthermore, Fe ($2p_{3/2}$), C (1s), O (1s) XPS lines at binding energies (710.3 ± 0.2 eV), (284.6, (C from adventitious carbon) 289.3 ± 0.1 eV), and (531.8 ± 0.2 eV) respectively signifies the presence of $FeCO_3$ corrosion product layer. Similar observation has been made earlier in the literature.[15-17]

Organic imidazoline inhibitor is characterized by its pendant chain and hydrocarbon tail. For better results the organic inhibitor must be chemisorbed (via pendant chain) on the metal surface to be effective.[18] Figure 10 (a) and (b) represents a high resolution N(1s) scan of full pipe and slug flow sample. The main peak (i) centered at 399.9 eV is from the main ring structure, whereas the peak at (ii) represents the N group from the pendant chain. Additional peaks featuring from 405.6 to 407.1 eV (noted as (iii) in Fig.10) at the left-hand side of the main peak are the prominent satellite peaks. The core level spectra of aromatic nitrogen containing polymeric molecules show similar shake up structures on the high binding energy side of the main photoelectron lines.[19] Discrete nature of the shake up satellites may also indicate the integrity of the organic molecule. It is this satellite peak of nitrogen (at ~ 406.2 ± 0.1 eV), which is more prominent in the full pipe flow than the slug flow thus indicating a possible disintegration and shearing of the inhibitor imidazoline molecule in the later. Thus the intensity of the N (1s) peak is significantly reduced in the slug flow (Fr = 6). The loss of N ring peak may be due to the imidazoline hydrolysis to amide; however, no significant growth of amide peak in the N spectrum (Figure 10 b) is noted. A possible peak at ~ 407.9 eV (N 1s: Fig 10 b, iv) may indicate the presence of sodium nitrate (Na 1s ~ 1071.8 eV from Fig 9 b) type compounds, a result of destruction of oleic imidazoline inhibitor due to slug flow conditions.[20,21]

CONCLUSIONS

The analysis of the corrosion product layers at different flow condition reveals a systematic topographic variation on the surface. Stacked iron carbonate crystals are seen in the full pipe flow, and the growth is enhanced as the fluid velocity is increased. The porosity increases with the flow velocity and is further enhanced in 20% oil by volume in oil and seawater. Higher velocities accompanied by high shear induce higher corrosion rates. This affects the thickness of the layer and removes the corrosion product layer. This results in the exposure of a bare metal surface, which further increases the corrosion rate. At higher

Froude numbers, the chances of a stable corrosion product layer is negligible. AFM measurements confirm a very rough surface in Froude 9 with respect to full pipe flow sample. XPS analysis of the surface shows presence of nitrogen in the uncorroded region, thus the inhibition action by imidazoline molecule. The total nitrogen is decreased from the full pipe to the slug flow. From the shape and nature of the N(1s) satellite peaks in full pipe and slug flow sample, one can detect the degradation of the inhibitor molecule as the flow is increased from full pipe to Fr = 6. The shake up satellite peaks from XPS N(1s) spectra are proved to be a definite means of determining the integrity of the organic inhibitor structure on C-steels used in oil and gas lines.

ACKNOWLEDGEMENT

Authors acknowledge NSF-I/UCRC Corrosion in Multiphase Systems Center, Ohio University and National Science Foundation (Grant No. 9907794) for supporting the current research work. Materials characterization was performed in the UCF-Cirent Materials Characterization Facility (MCF) founded by Advanced Materials Processing and Analysis Center (AMPAC). The corrosion coupons were exposed in high-pressure horizontal multiphase flow loop at Ohio University.

REFERENCES

1. K. Videm, A. Dugstad, Envorinmental Treatment and Control, (1986), p 63.

2. G. Ogundale and W. E. White, *Corrosion* 42: 2, 71 (1986).

3. T. L. Webb and J. E. Kruger, *Differential Thermal Analysis*, Vol. 1, Fundamental Aspects ed., R.C. Hackenzie, p. 327, Acad. Press, New York (1970).

4. A. K. Vappu, *Masters Thesis*, Ohio University (1994).

5. Z. Fan, W. P. Jepson and T. J. Harratty, *Inst. J. Muitiphase Flow*, 18, 4, 447 (1992).

6. A. D. Mercer, Corrosion, 2nd ed., Vol 2, p. 18, L.L. Schrier, Buttsworth, Sevenoater, Kent, England (1976).

7. A. Edwards, C. Osborne, S. Webster, D. Klenerman, M. Joseph, P. Ostorer and M. Doyle, Corrosion Science 30 (1994) 315.

8. A. J. Mchohan, Colloids and Surfaces 59 (1991) 187.

9. A. J. Mchohan, Proc. 7th European Symp. Corrosion Inhibitors, University of Ferrara, Italy, (1990) pp. 1281.

10. T. L. Barr and S. Seal, J. Vac. Sci. Tech. A13, 1239 (1995).

11. T. Hong, Advisory Board Meeting, Ohio university, 1999.

12. C.A. Palacios and J.R. Shadley, " Characteristics of corrosion scales on steel in a CO_2 saturated NaCl Brine ", Corrosion, vol. 47, No.2. 1991, p122-127.

13. B. Kinsella, Y.J. Tan, and S. Bailey, electrochemical Impedance Spectroscopy and surface characterization techniques to Study Carbon Dioxide Corrosion Product Scales, Corrosion, vol. 54, No.10, 1998, p835-842.

14. J. K. Heuer and J. F. Stubbins, *Corrosion*, 54, No. 7, 566 (1998).

15. D. Briggs and M. P. Seah, Practical Surface Analysis, John Wiley & Sons, NY, 1990.
16. P. Mills and J. L. Sullivan, J. Phys.D. App. Phys. 16 (1983) 723.

17. J. F. Moulder, W. F. Stickle, P. E. Sobol and K. D. Bomben, Handbook of X-ray Photoelectron Spectroscopy, Perkins-Balmer Corporation, Eden Praire, Minnesota, 1995.

18. A. J. Mchohan, Colloids and Surfaces 59 (1991) 187.

19. G. Beamson and D. Briggs, High Resolution XPS of Organic Polymers, J Wiley and Sons, Chichestor, England, 1992.

20. S. Seal, N. Sobezak, S. J. Kerber, T. L. Barr, J. Materials Science, 33 (1998) 4147.

21. K. Burger, F. Tschismarov, H. Ebel, J. Elec. Spec. Rel. Phen. 10 (1977) 461.

TABLE 1
Porosity measurements of stainless steels at multiphase flow condition.

Samples	Aspect Ratio	Mean Hole Area	Mean Roundness	% Porosity
		Sq. micrometers		
Full Pipe Flow 100% water cut	2.44	0.0125	1.69	5.7
Slug Flow Fr. No.6 100% water cut	2.39	0.215	2.4	24.3
Slug Flow Fr. No.9 100% water cut	2.4	0.1019	1.49	29.9
Slug Flow Fr. No.9 80% water cut	2.32	0.1724	1.44	31.3

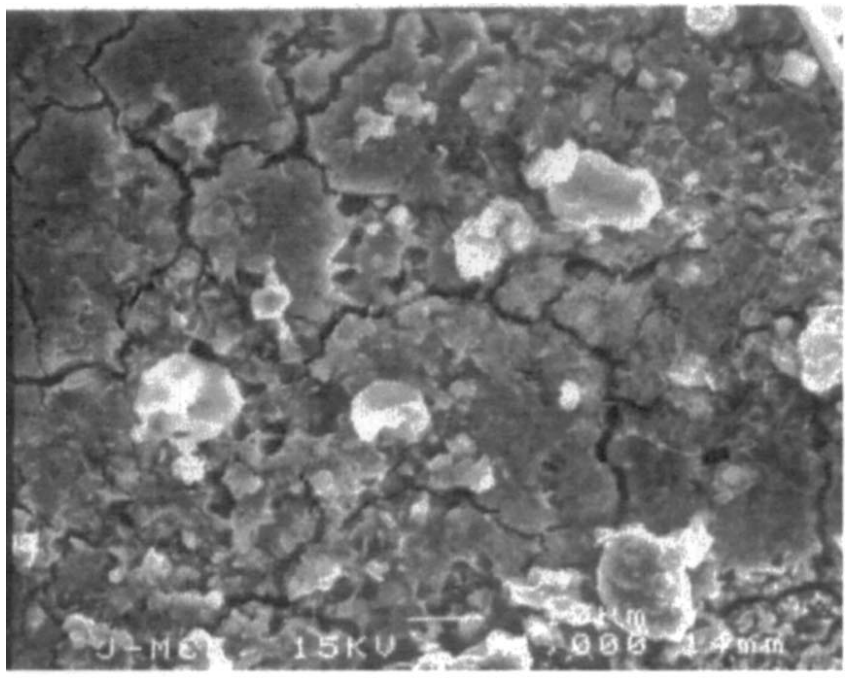

(a)

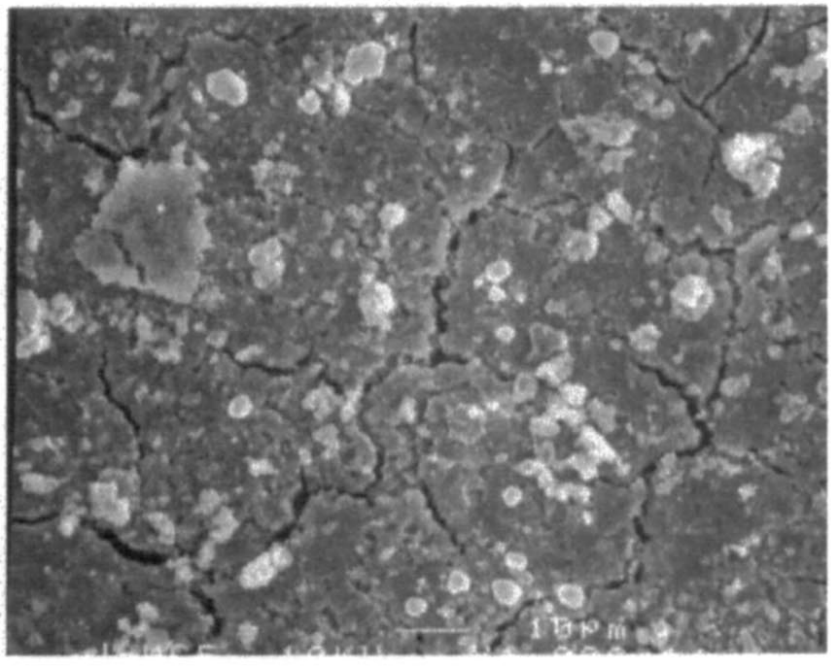

(b)

Figure 1. SEM micrograph of steel coupons at full pipe flow (a) 0.55m/s, (b) 1.1 m/s, (c) 1.5 m/s and (d) 1.5 m/s zoom in view. Exposure time 24 hours.

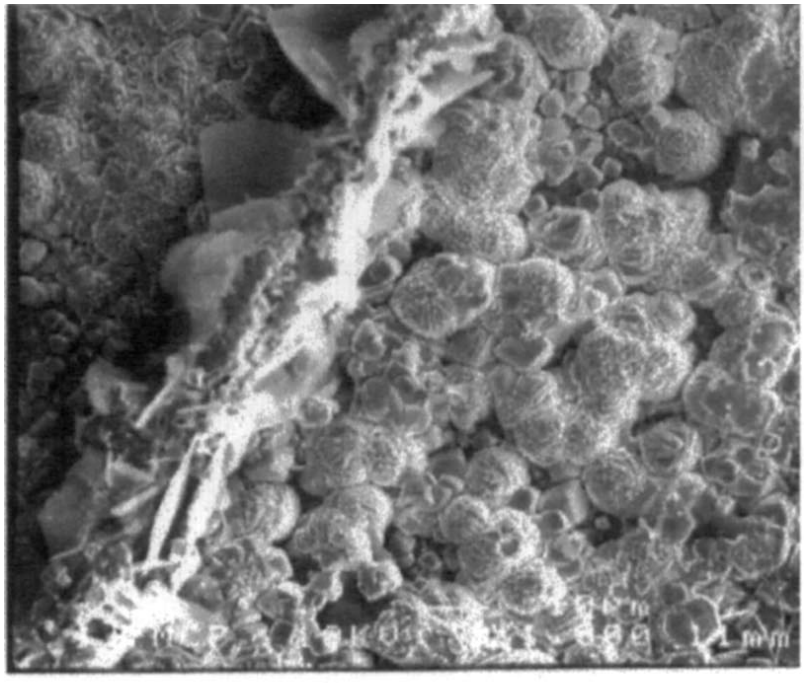

(c)

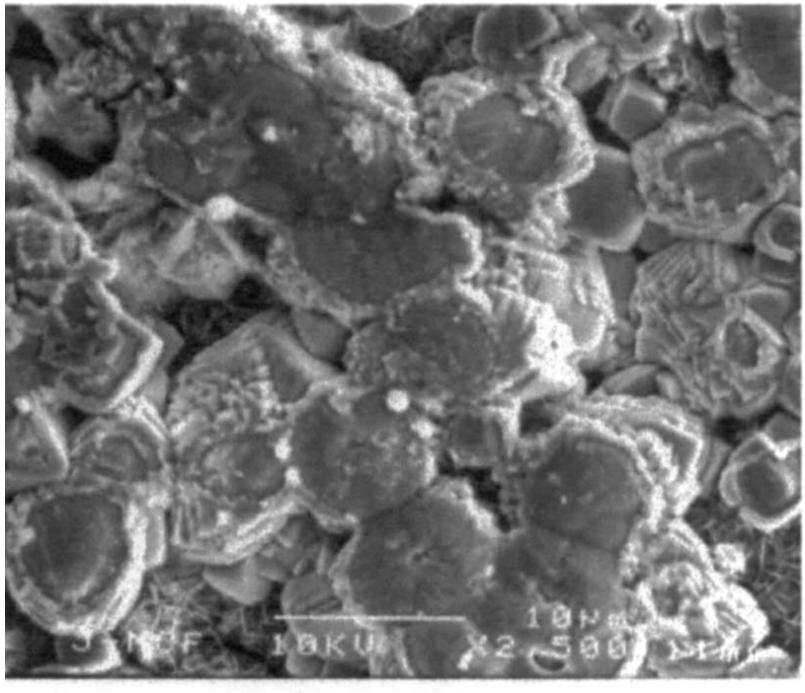

(d)

FIGURE 1 - SEM micrograph of steel coupons at full pipe flow (a) 0.55m/s, (b) 1.1 m/s, (c) 1.5 m/s and (d) 1.5 m/s zoom in view. Exposure time 24 hours.

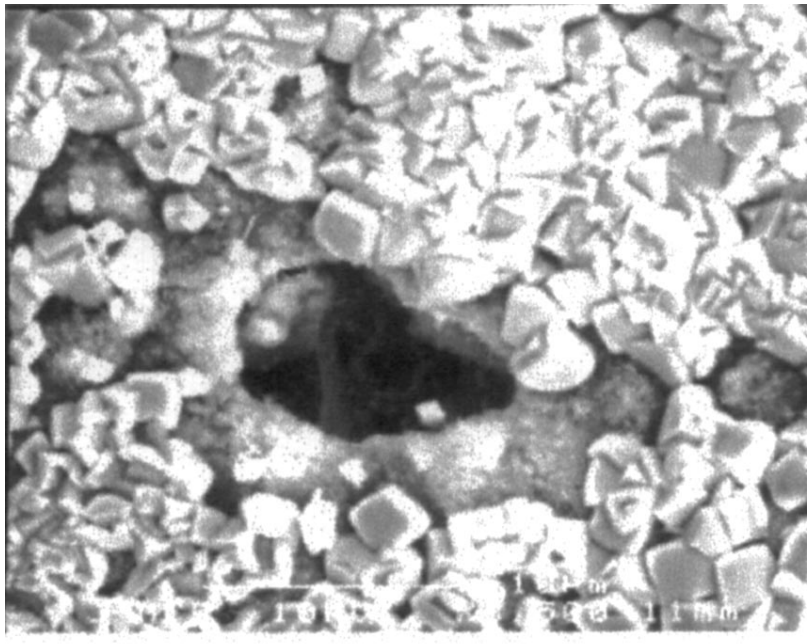

(a)

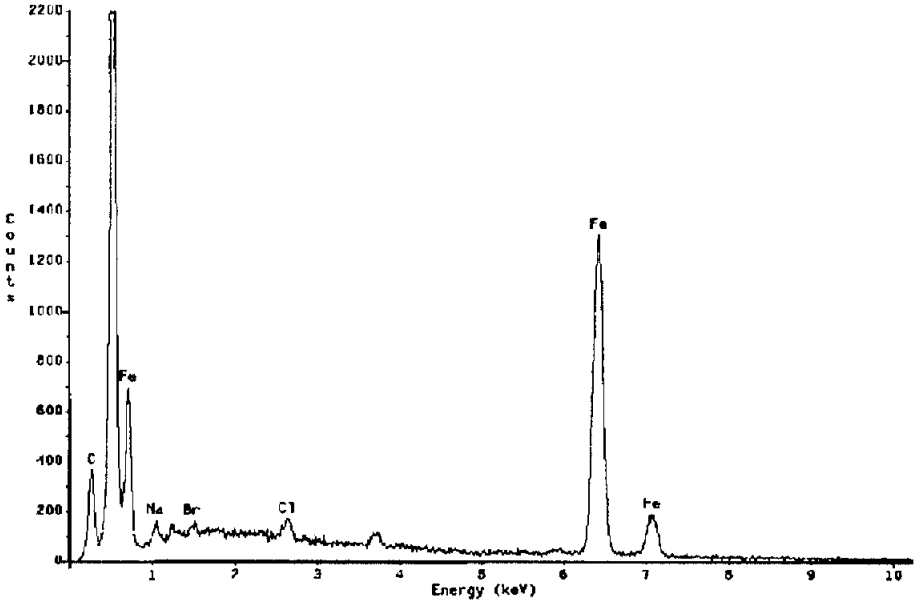

(b)

FIGURE 2 - SEM micrograph of steel coupons (a) Froude no. 6 and (b) corresponding EDX spectra, exposure time 5 hours.

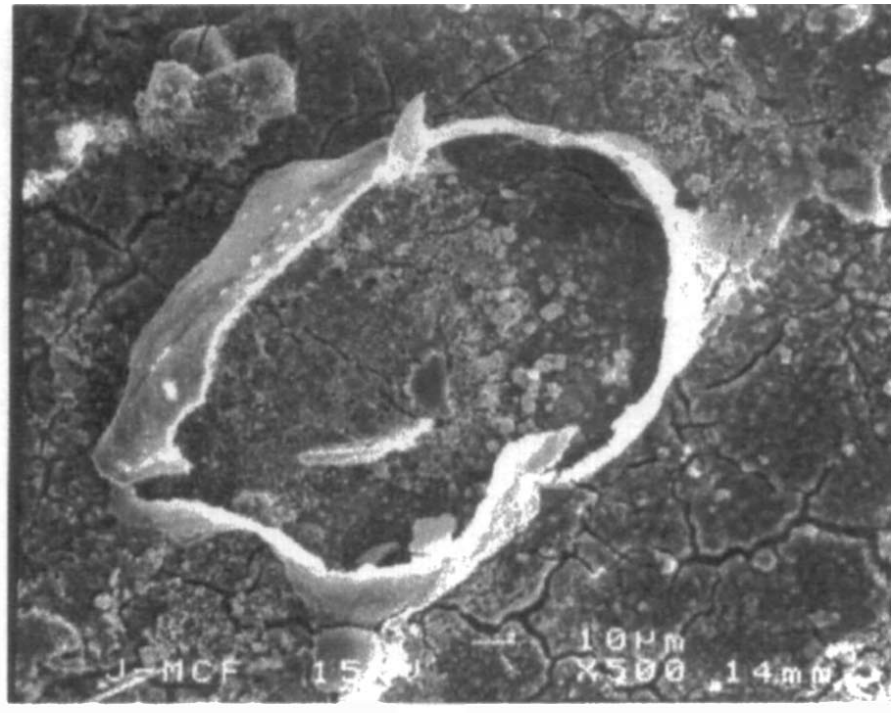

(a)

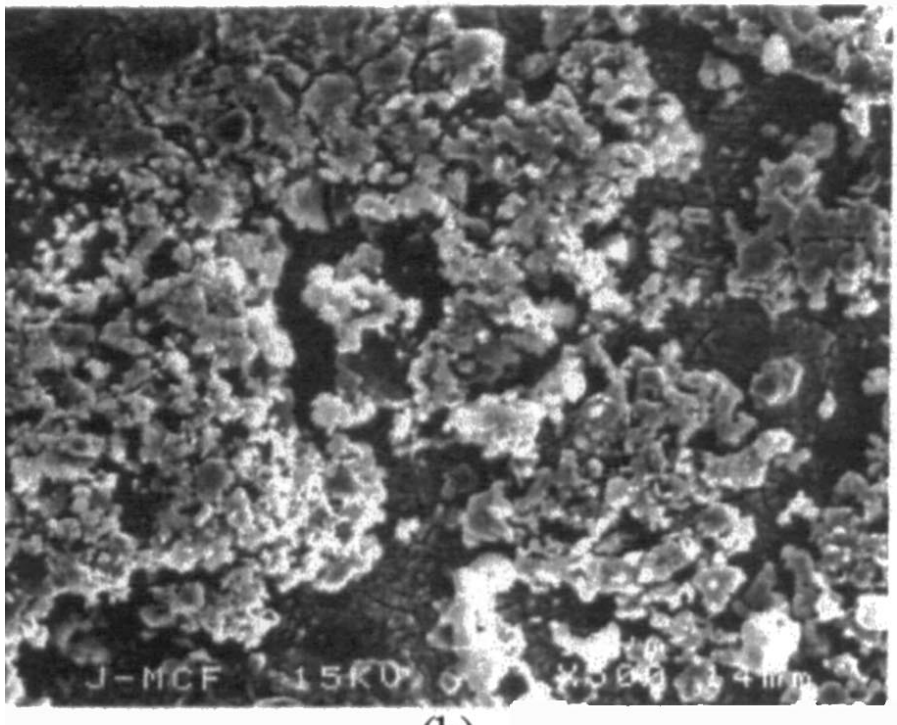

(b)

FIGURE 3 - SEM micrograph of steel coupons at Froude no. 9 (a) showing bubble impact and (b) porous surface inside the bubble region. Exposure time 5 hours

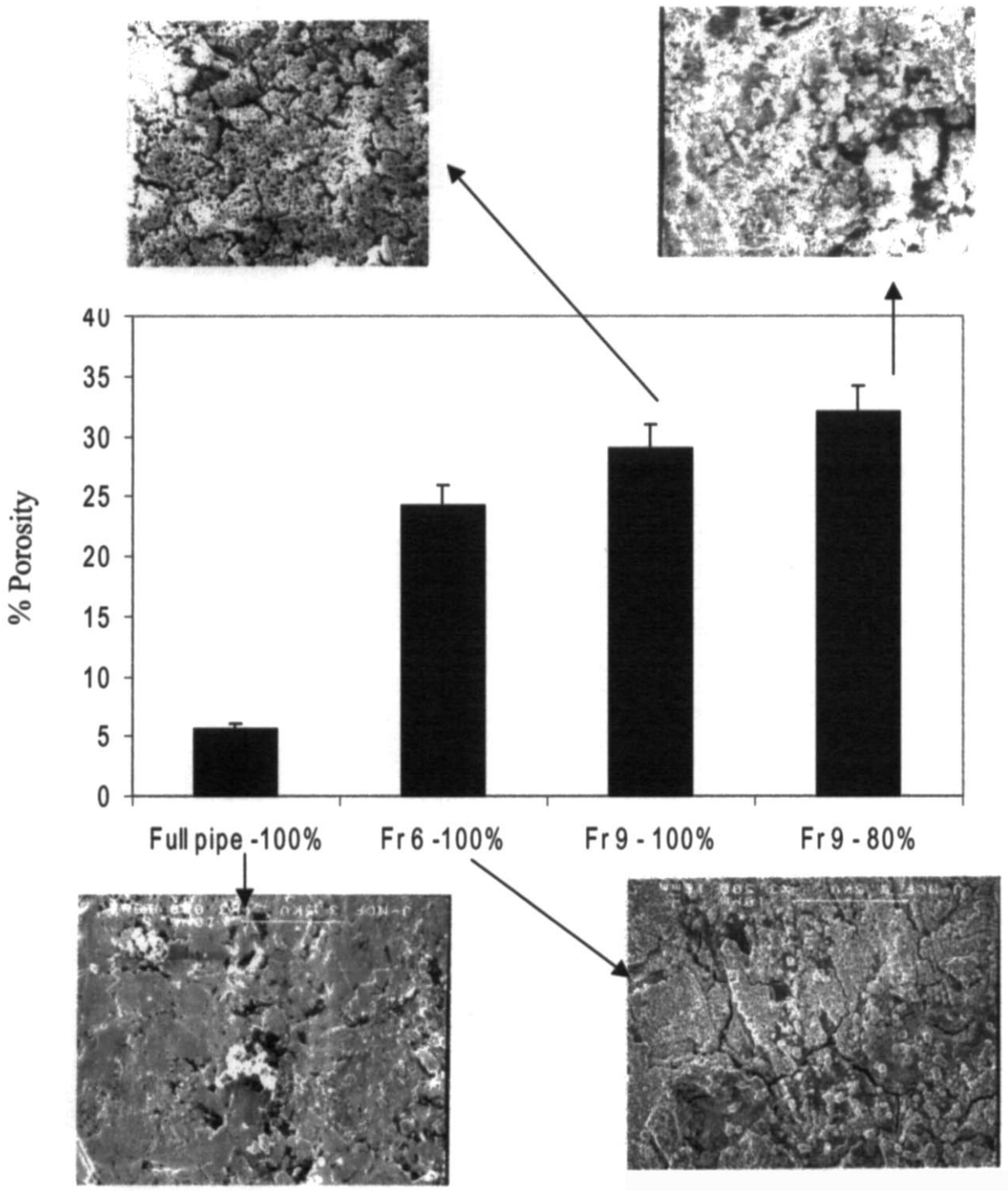

FIGURE 4 - Porosity values measured on full pipe flow (1 m/s) and slug flow samples with Froude numbers 6 and 9. The liquid fluid compositions are 0% (100% watercut) and 20% oil (80% watercut) by volume in oil and seawater.

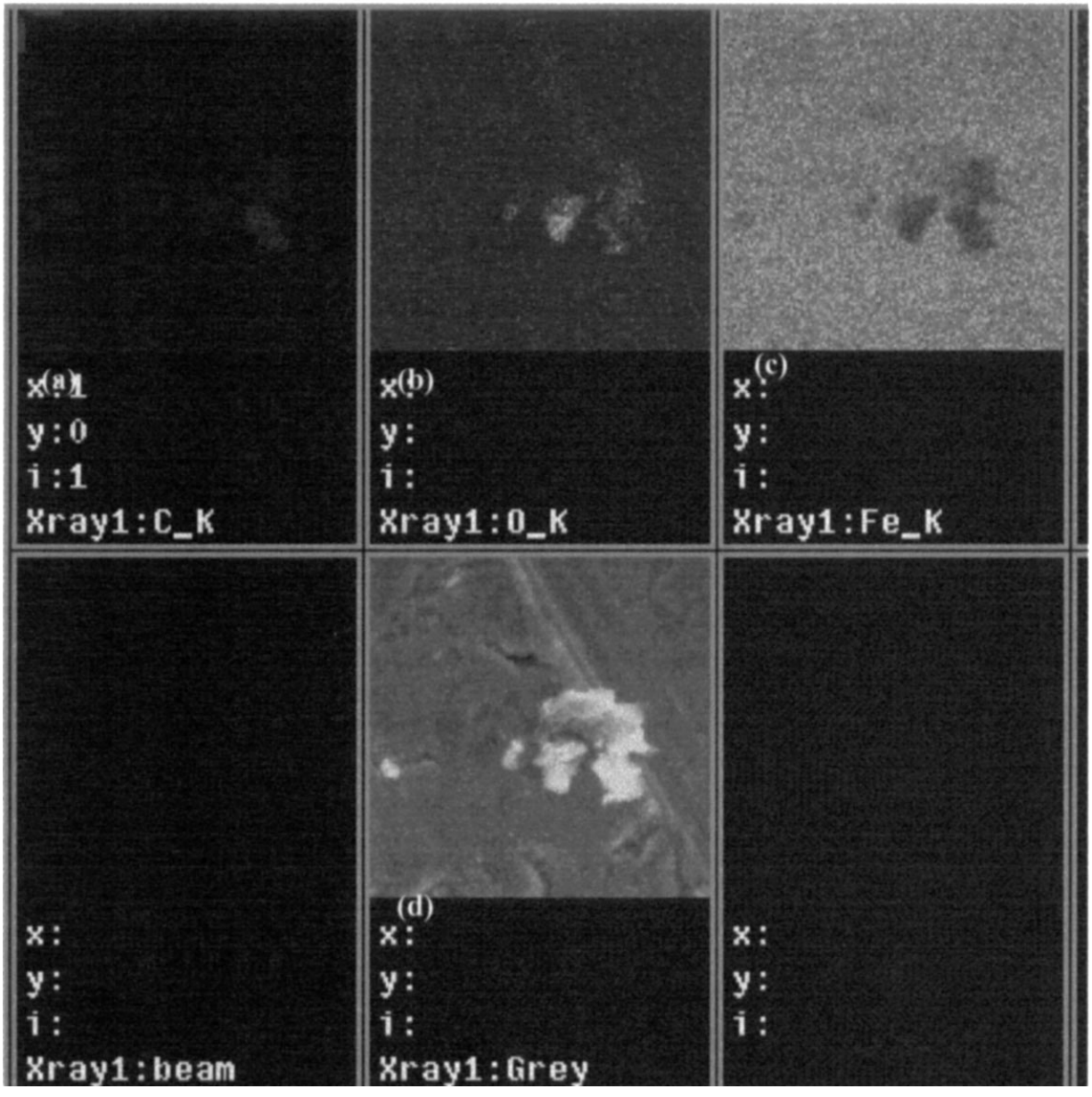

FIGURE 5 - X-ray mapping (a) C map, (b) O map, (c) Fe map and (d) SEM micrograph iron carboante formation on 1018 steel.

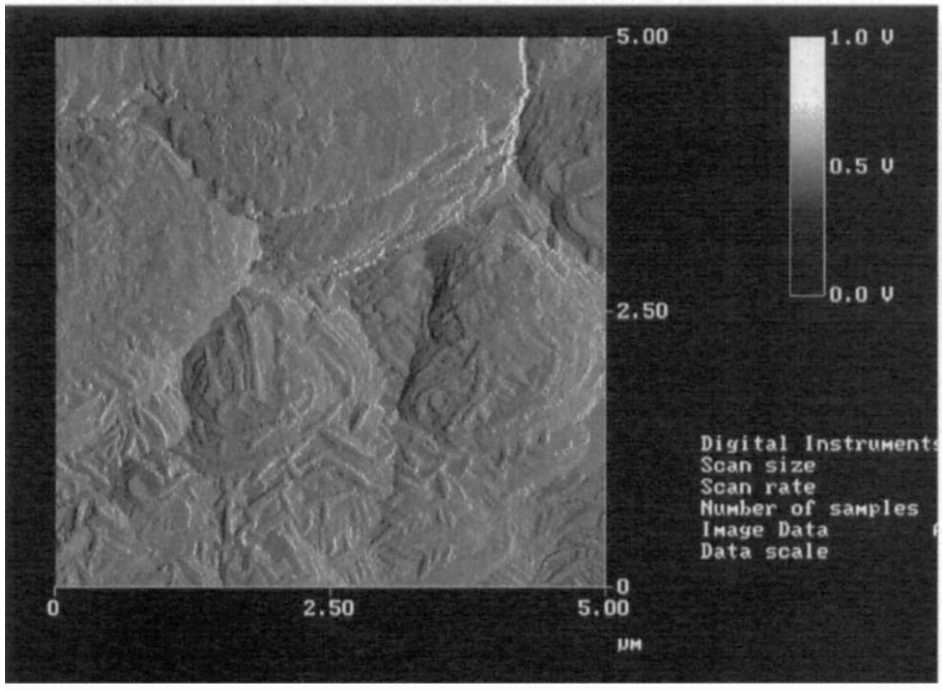

(a)

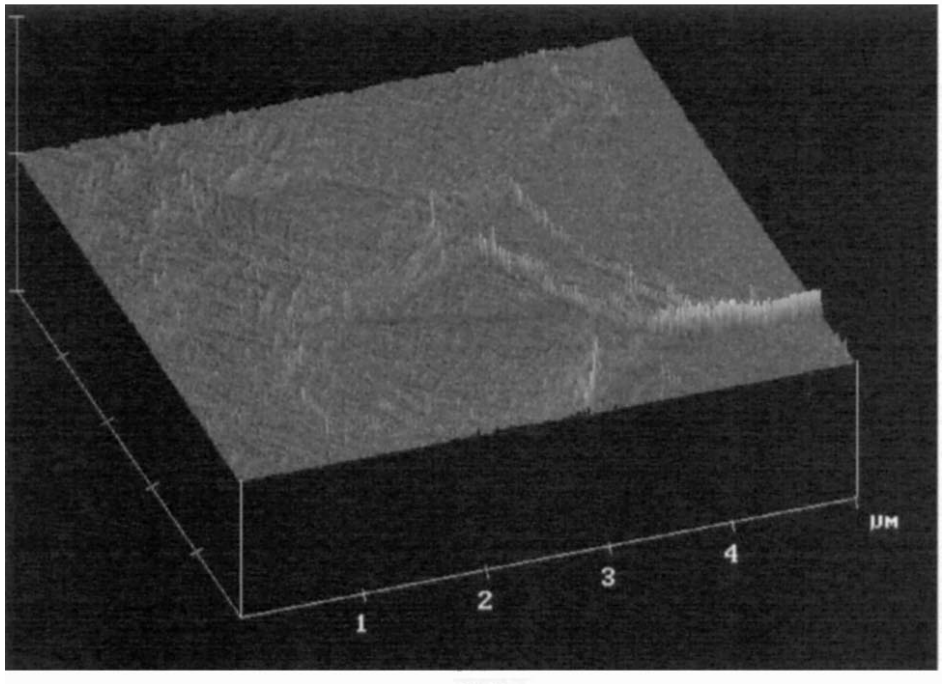

(b)

FIGURE 6 - AFM images of full pipe sample (0.55 m/s) (a) 2D and (b) 3D.

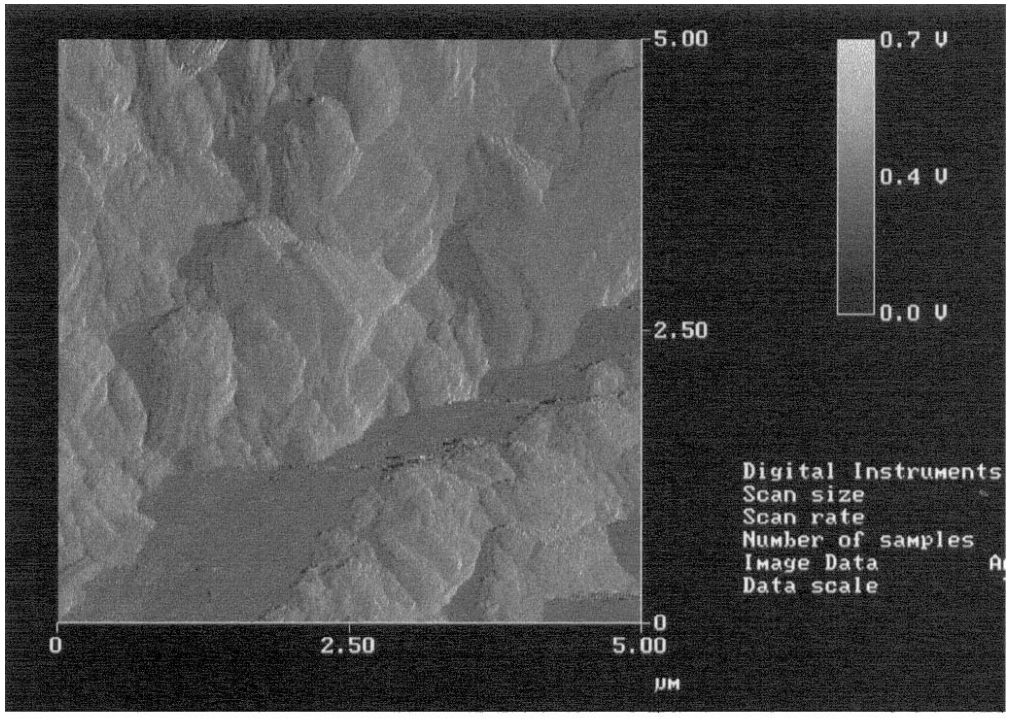

(a)

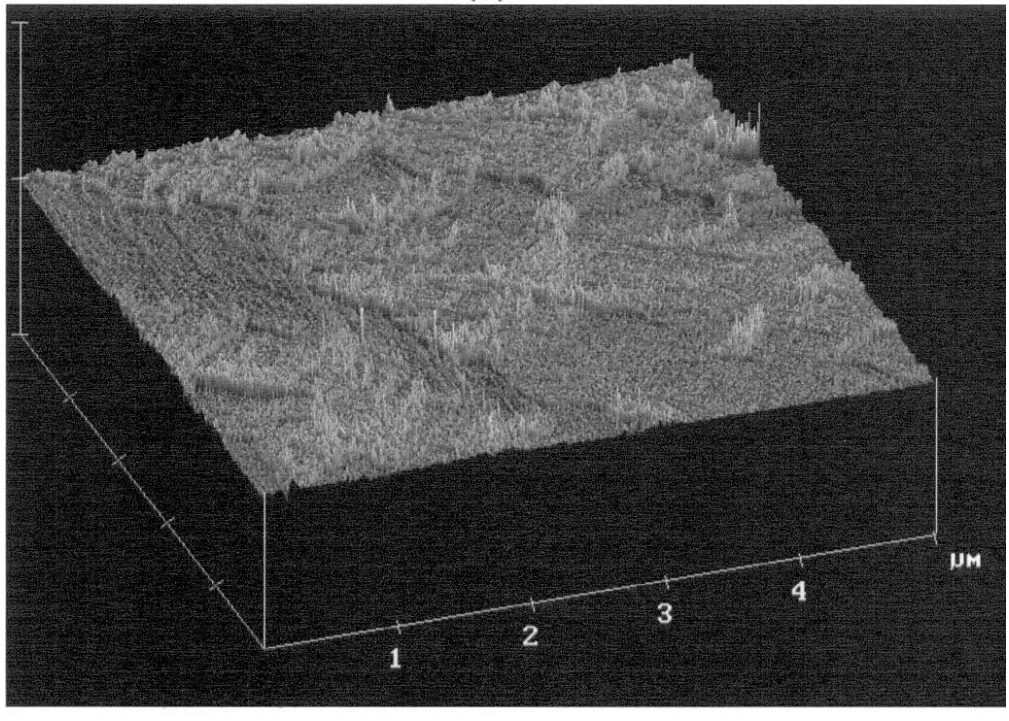

(b)

FIGURE 7 - AFM images of slug flow sample, Froude no. 9 (a) 2D and (b) 3D.

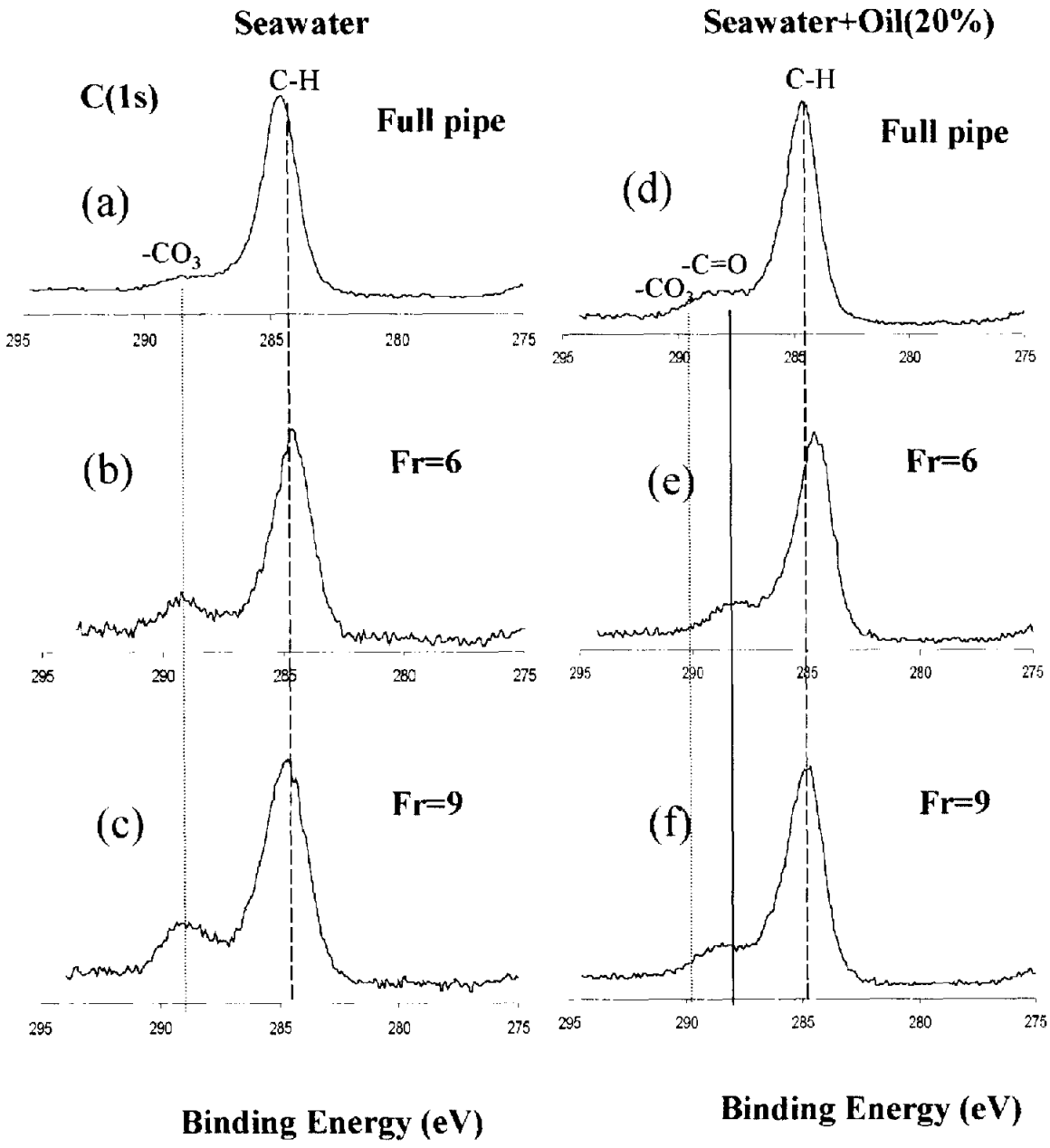

FIGURE 8 - Comparisons between the carbon peaks in Full pipe, Froude 6, Froude 9 flow conditions.

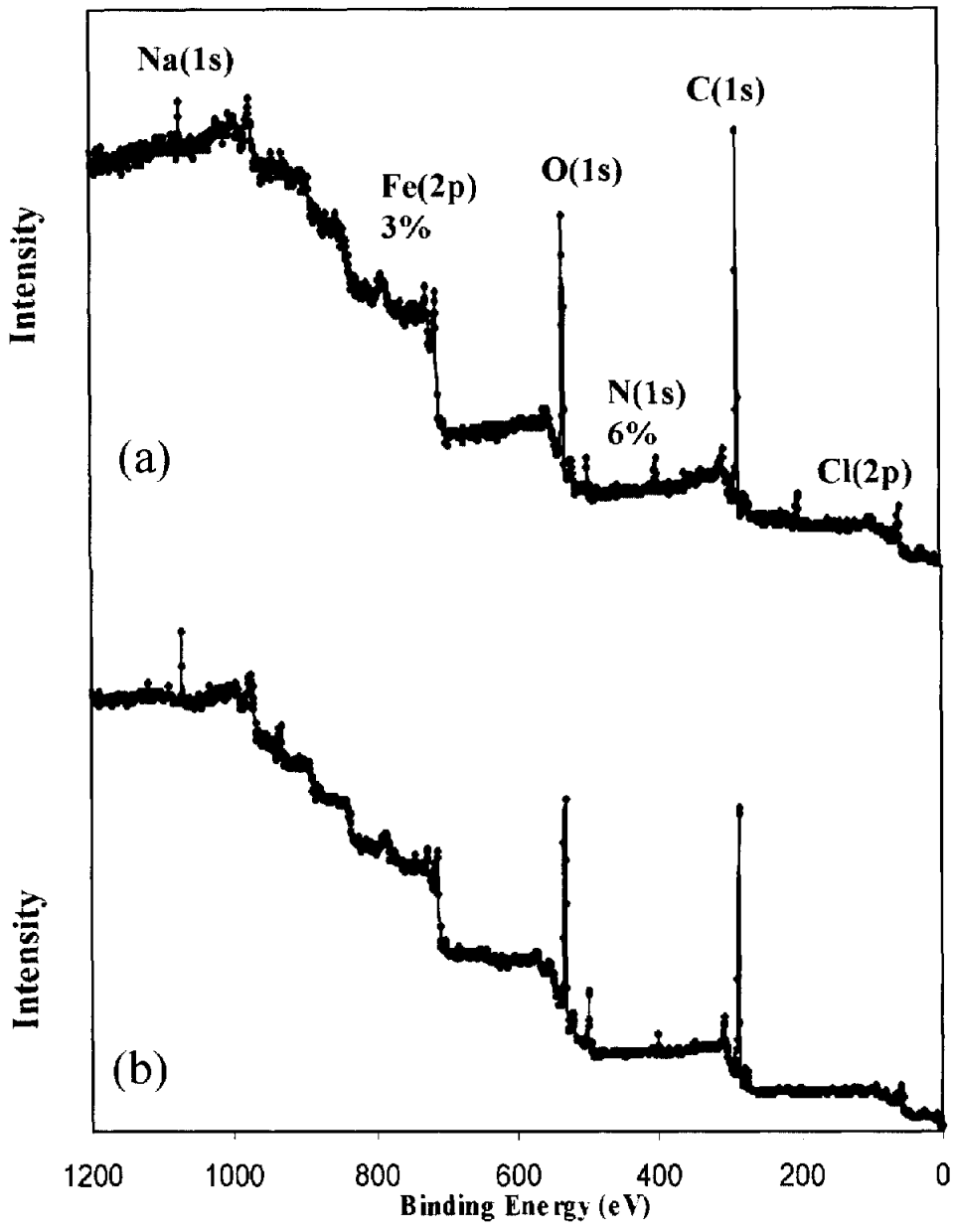

FIGURE 9 - XPS survey (0-1200eV) spectrum
(a) full pipe flow
(b) slug flow (Fr. No. 6)
Note: Nitrogen content is higher in (a) wrt. (b) indicating the destruction of imidazoline inhibitor.

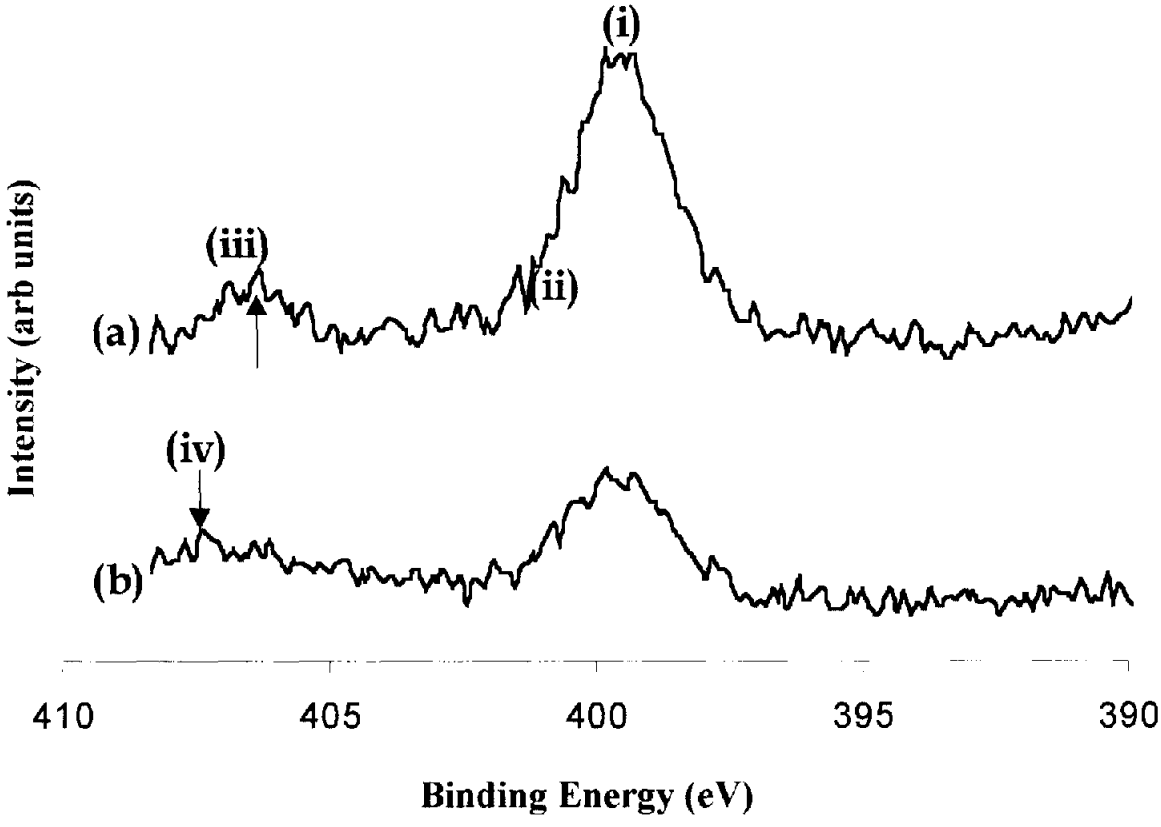

FIGURE 10 - N(1s) XPS spectra for 1018 C-steel specimen subjected to (a) Full pipe flow and (b) Slug pipe (Fr. No. 6) (i), (ii) and (iii) are discussed in the text. Note: Satellite peaks (iii) are more prominent in (a) than (b), arrow indicating possible presence of nitrates.